THE TRAPPED RADIATION HANDBOOK

JOHN B. CLADIS, ET AL

LOCKHEED PALO ALTO RESEARCH LABORATORY
PALO ALTO, CALIFORNIA

DECEMBER 1971

which is comparable with the gravitational drift velocity of protons (Equation 3-32).

3.3.2 Magnetic Reflection

Generally, a nonhomogeneous magnetic field has regions where the field lines converge. In those regions, the magnetic force $(q/c)\bar{v} \times \bar{B}$ has a small component directed along the field lines. This component tends to deflect a charged particle away from a region of increasing field strength.

The magnetic force components are depicted in Figure 3-9. The relative magnitudes of the force components are variable. Usually the centripetal force is the major part of the magnetic force. When the retarding force along the field lines is relatively weak, the equation of motion yields an acceleration (or deceleration) in the field direction $\bar{B}$ (References 4 and 21):

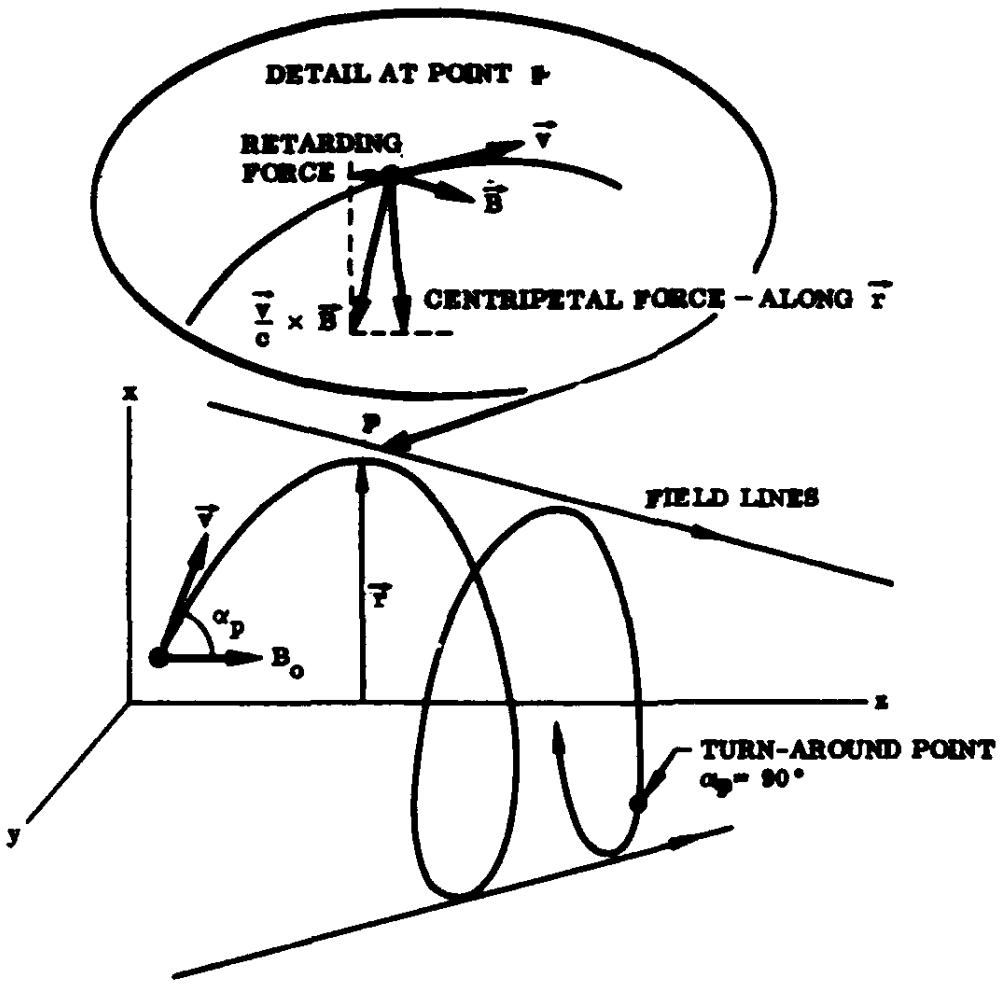

Figure 3-9. Components of the force acting on a positively charged particle in a converging magnetic field.

$$\frac{dv_{\parallel}}{dt} \cong - \frac{1}{2} \frac{v_{\perp}^2}{\gamma B} \frac{d\bar{B}}{dS} \qquad (3\text{-}41b)$$

to first order in the variation of B with distance S along the field line. The similarity to the drift velocity Equation 3-37 especially should be noted. Here, too, gravitational effects are comparable with the field inhomogeneity effects for thermal velocity protons.

The radial component of the equation of motion reduces to:

$$\frac{dv_{\perp}}{dt} \cong \frac{1}{2} \frac{v_{\parallel} v_{\perp}}{\gamma B} \frac{dB}{dS} \quad . \qquad (3\text{-}42)$$

But $v_{\parallel}\, dB/dS$ is just the time rate of change of magnetic field intensity as experienced by a spiraling particle. Equation 3-42 therefore yields the simple relation:

$$v_{\perp}^2 \propto B \quad . \qquad (3\text{-}43)$$

Charged particles in a converging magnetic field travel toward the "ends" of the field only as far as the turnaround or mirror points (Reference 1) where $p_{\perp}^2$ is equal to p^2, the total momentum squared. This definition of the turnaround points is not in exact accord with Section 3.2.3. For all practical purposes, the turnaround point is regarded simply as the location where there is no component of momentum along the general direction of the field. To avoid confusion, the term mirror point will be used here except when the specific meaning of Section 3.2.3 is intended.

If the magnetic field is closed at two ends, charged particles will continue to "bounce" back and forth until they either lose energy or are deflected by some external process. Figure 1-3 shows how charged particles move in the earth's field (ignoring drift motion).

It is convenient to define the pitch angle α_p as the angle between the particle's momentum and the magnetic field (some of the early literature on magnetic trapping refers to the pitch angle as the complement of the angle defined here). The pitch angle is indicated in Figures 1-3 and 3-9. Equation 3-43 is equivalent to a simple relation which gives, at any point, the pitch angle variation in a magnetic field:

$$\sin \alpha_p = \sqrt{B/B_m} \qquad 3\text{-}44$$

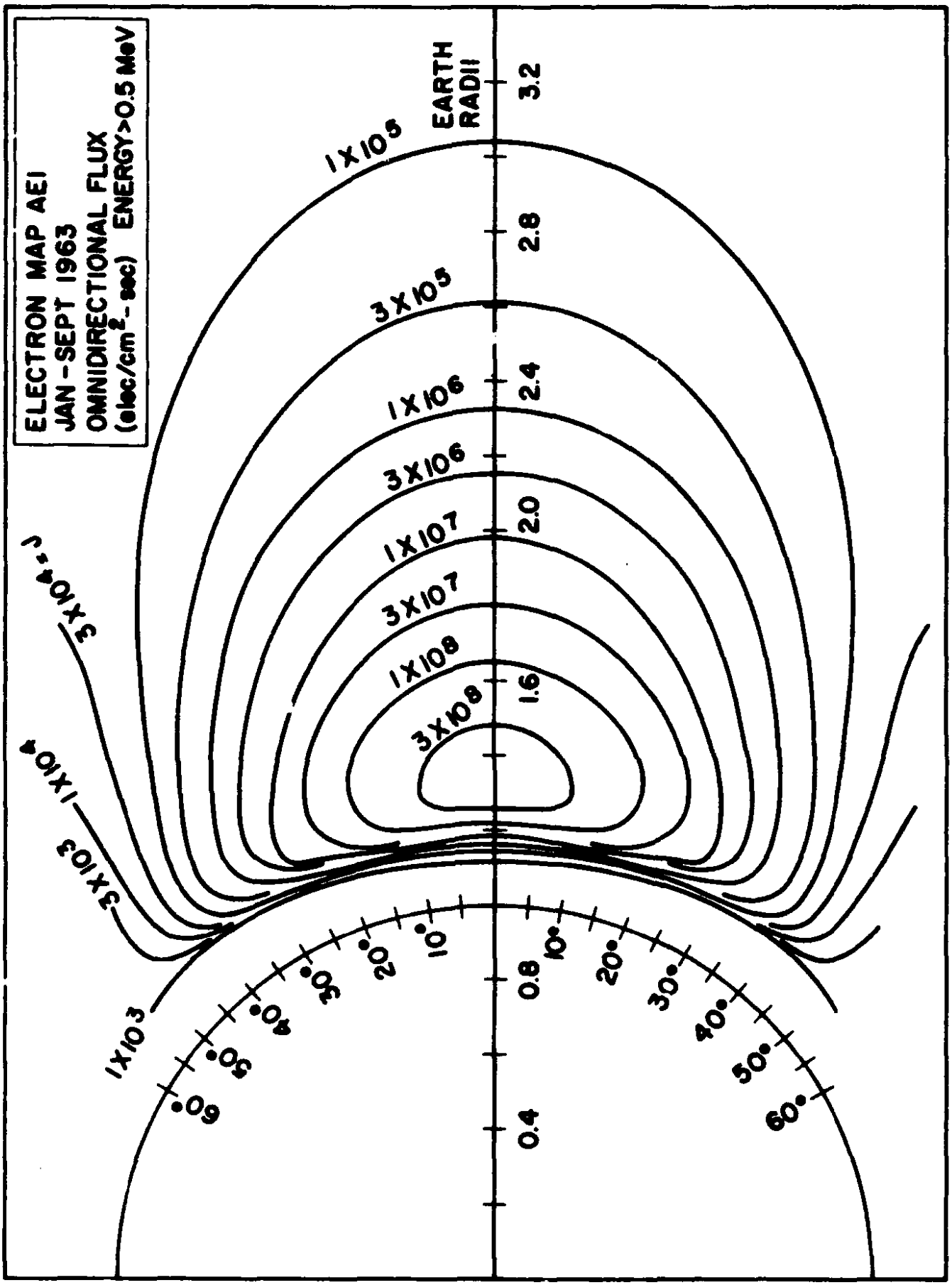

Figure 4-16. Post-Starfish electron flux map.

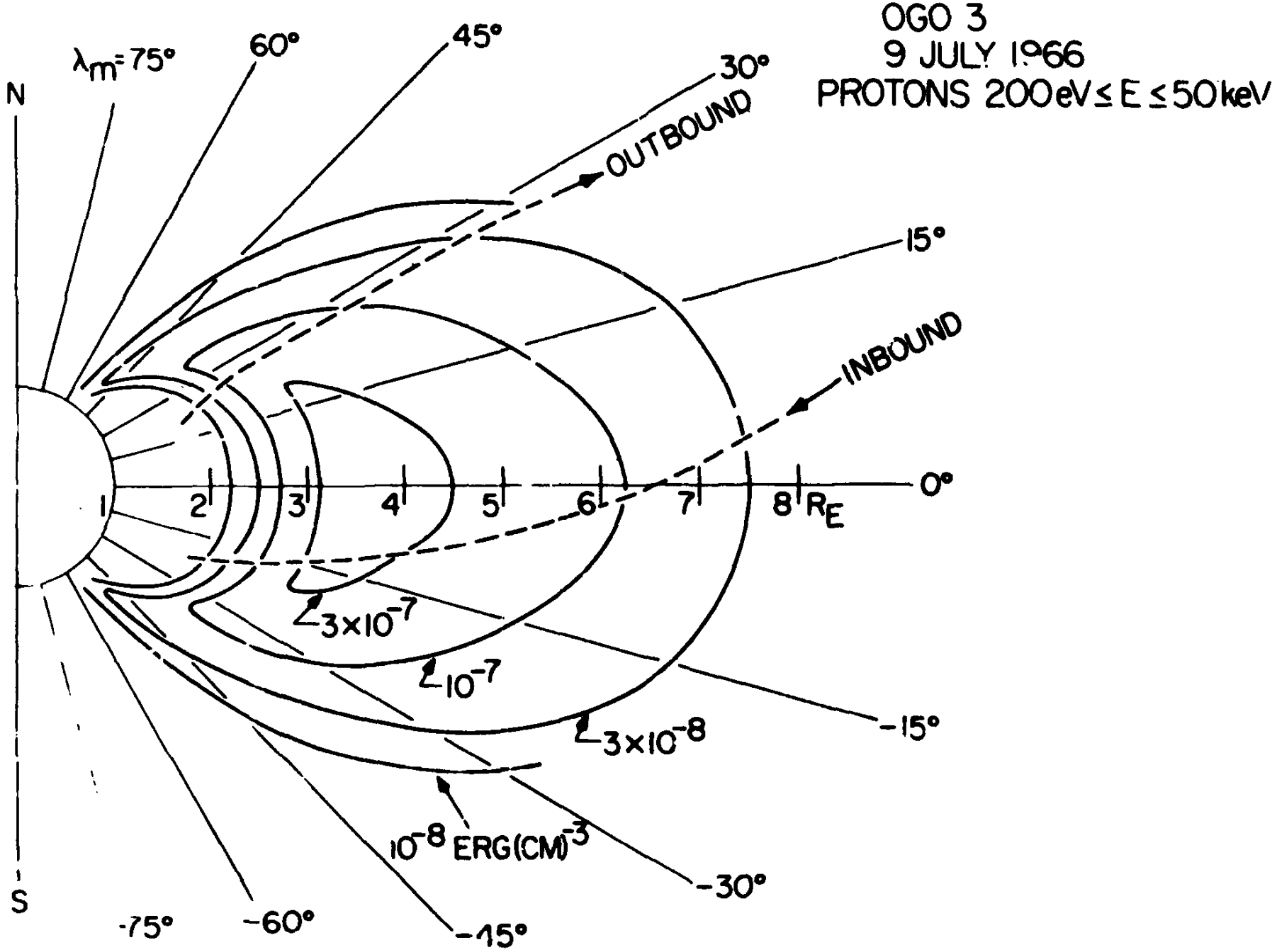

Figure 4–38. Distribution of very low-energy protons during a magnetic storm.

in late 1962 and 1963 in low-altitude orbits. However, these data are not particularly useful because of the restricted spatial coverage and short satellite life.

Table 6-8 lists the satellites that, to date, have given the most valuable information on the Starfish belt. Because of the widespread distribution of Starfish electrons and their long lifetimes, many other measurements of the belt have been made in conjunction with other space experiments.

6.4.3 Characteristics of the Starfish Belt

The complete description of the Starfish radiation belt perhaps never will be known since some of the needed early-time experimental data are lacking. This summary, which is based primarily on satellite observations of trapped particles, will present all available information in a concise form. Comments on the injection mechanisms will be given in Section 6.4.5.

Following the Starfish explosion, an intense radiation belt was formed. The contours of the belt (Figure 6-15) as determined by

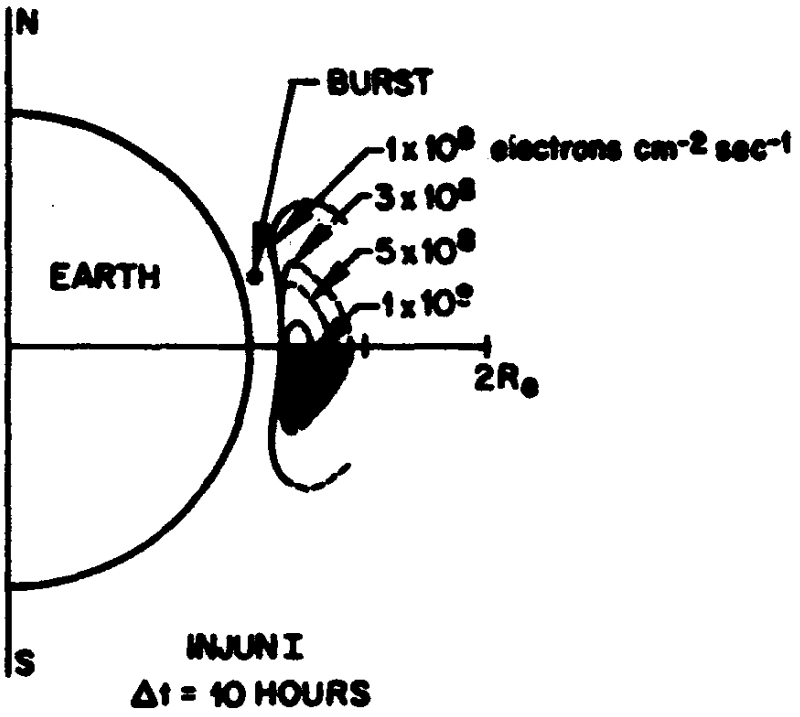

Figure 6-15. Flux contours 10 hours after Starfish, as determined from Injun I data.

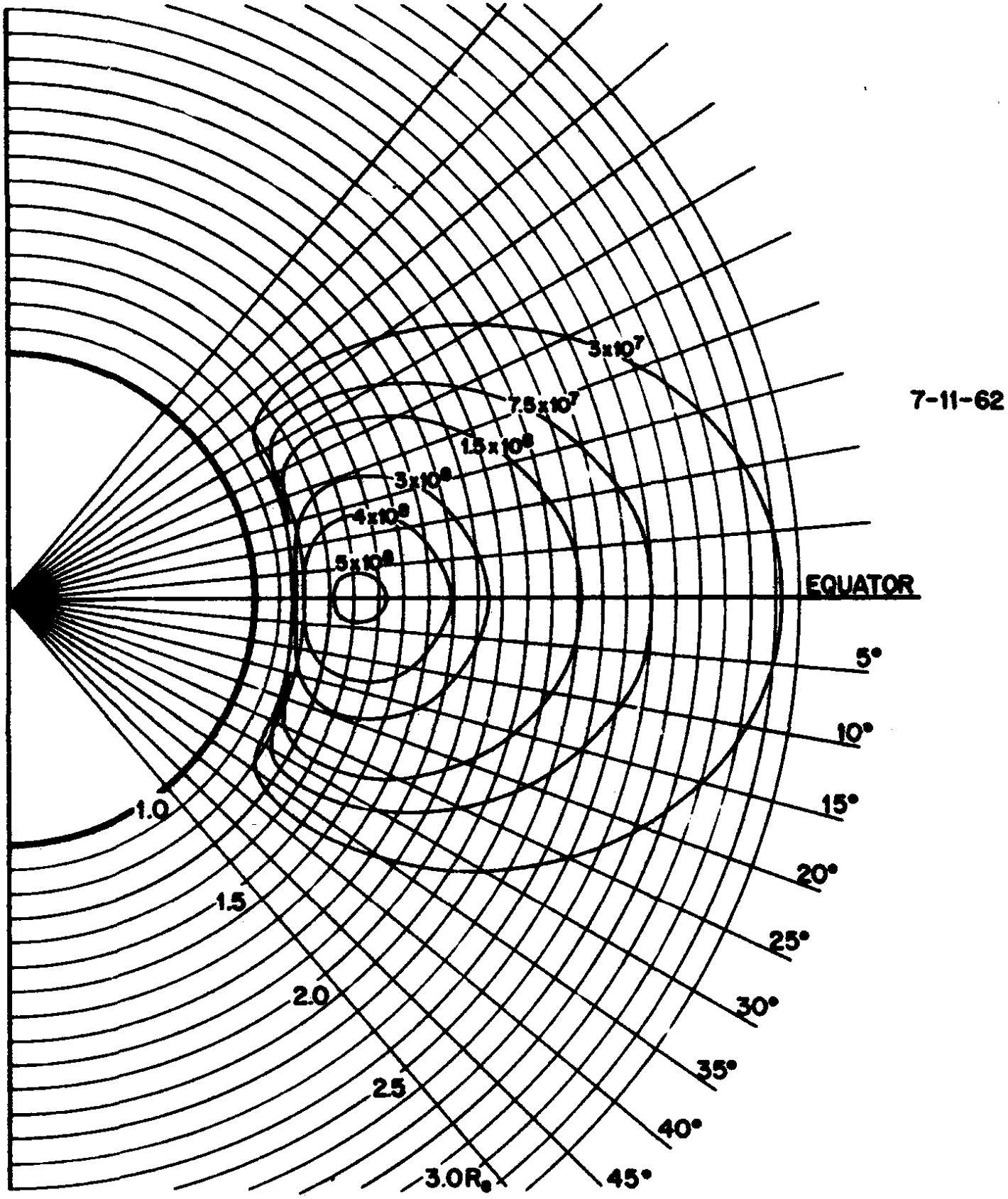

Figure 6-16. Flux contours 2 days after Starfish, as determined from Telstar data by Newkirk and Walt (unpublished).

The Cosmos 5 results do not support this explanation, however. The flux contours based on a low-energy electron detector (estimated energy sensitivity is in the range 15 to 50 KeV) show a very narrow maximum at about $L = 1.2$ and resemble the Injun I contours more closely than those of Telstar. The Cosmos 5 data have been discounted largely in the present analysis because (1) the energy sensitivity of the detector is uncertain, (2) the spatial coverage is very incomplete and some of the extrapolations performed by the original authors are clearly in error, i.e., assumption of flux independent of B, and (3) the incomplete nature of the published report makes it difficult to evaluate the probable errors in the smoothed results. The alleged maximum at $L = 1.2$ is based entirely on a 20-percent reduction in the flux in going from about $L = 1.2$ to 1.21. Thus, a 20-percent error in this region would vitiate the conclusion.

The various estimates of the inventory of electrons artificially added to the belts by the Starfish detonation are listed in Table 6-9. Choosing the best value for the total number of electrons injected by Starfish involves a subjective judgment. Furthermore, since some of the low-energy electrons may be ambient ionospheric electrons that were shock heated to relativistic energies, calculations of the injection efficiency may be meaningless. However, until further data are available, the inventory figure of 7.5×10^{25} recomputed from Telstar data is preferred as the best estimate of the actual inventory. Also, pending further theoretical analyses, the lower energy electrons at $L > 1.5$ are identified as fission electrons that were transported across L-shells by a flute instability or some other electromagnetic effect. Thus, the total number of injected electrons is taken to be 7.5×10^{25}, giving an injection efficiency of about 10 percent.

6.4.4 Decay of the Starfish Radiation Belt

The decay of the Starfish radiation belt has been studied extensively and an enormous body of data has been accumulated. From these data have come the best information to date on the dynamics of trapped electrons at $L \lesssim 2$. In general, the decay is complex—it is not a true exponential and changes more rapidly at early times. Examples of the observed decay are shown in Figure 6-19 from Injun I and Injun III data, and Figure 6-20 from Telstar data. Pre-Starfish background rates in Figure 6-19 are shown by the horizontal bars (Reference 25). Although the decay is not exponential, it has been convenient to approximate the time variation by an exponential function and to designate the lifetime as the time required for the flux to decrease a factor of $1/e$. This

Explorer 14 would not have detected a flux of the magnitude seen by Alouette at $L > 3.6$. Hence, injection probably did occur to about $L = 6$. A double maximum in the L-profile of the belt was suggested by Alouette's data. This observation was confirmed by passes of Explorer 15 made shortly before the second Russian shot.

The most complete flux distributions for this event were derived from Telstar's counting rates (Reference 56). A plot of omnidirectional fluxes in R, λ coordinates is shown in Figure 6-23. The dotted

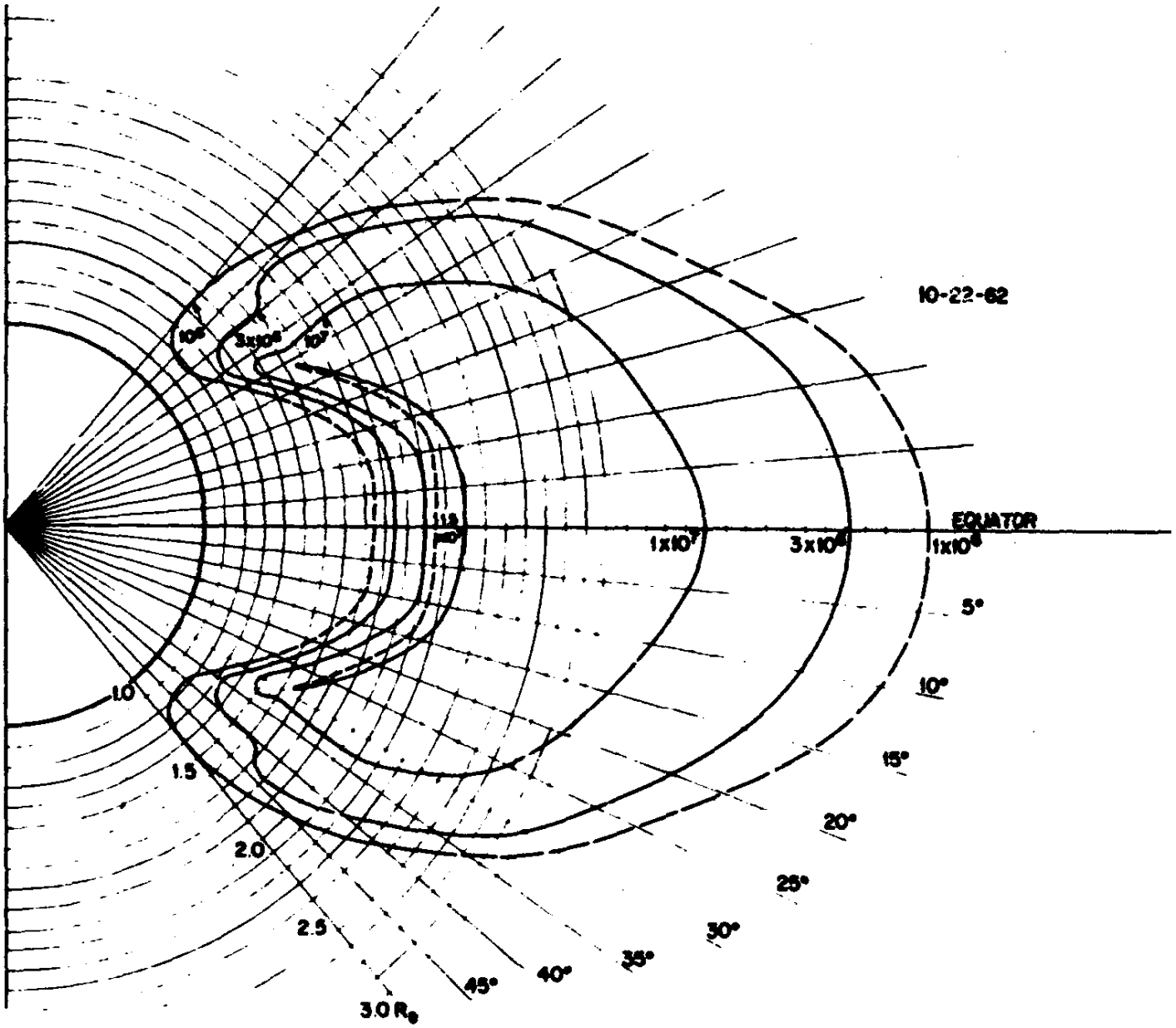

Figure 6-23. Omnidirectional flux (cm^{-2} sec^{-1}) contours (Telstar data) immediately following the Russian test of 22 October 1962 (Reference 56).

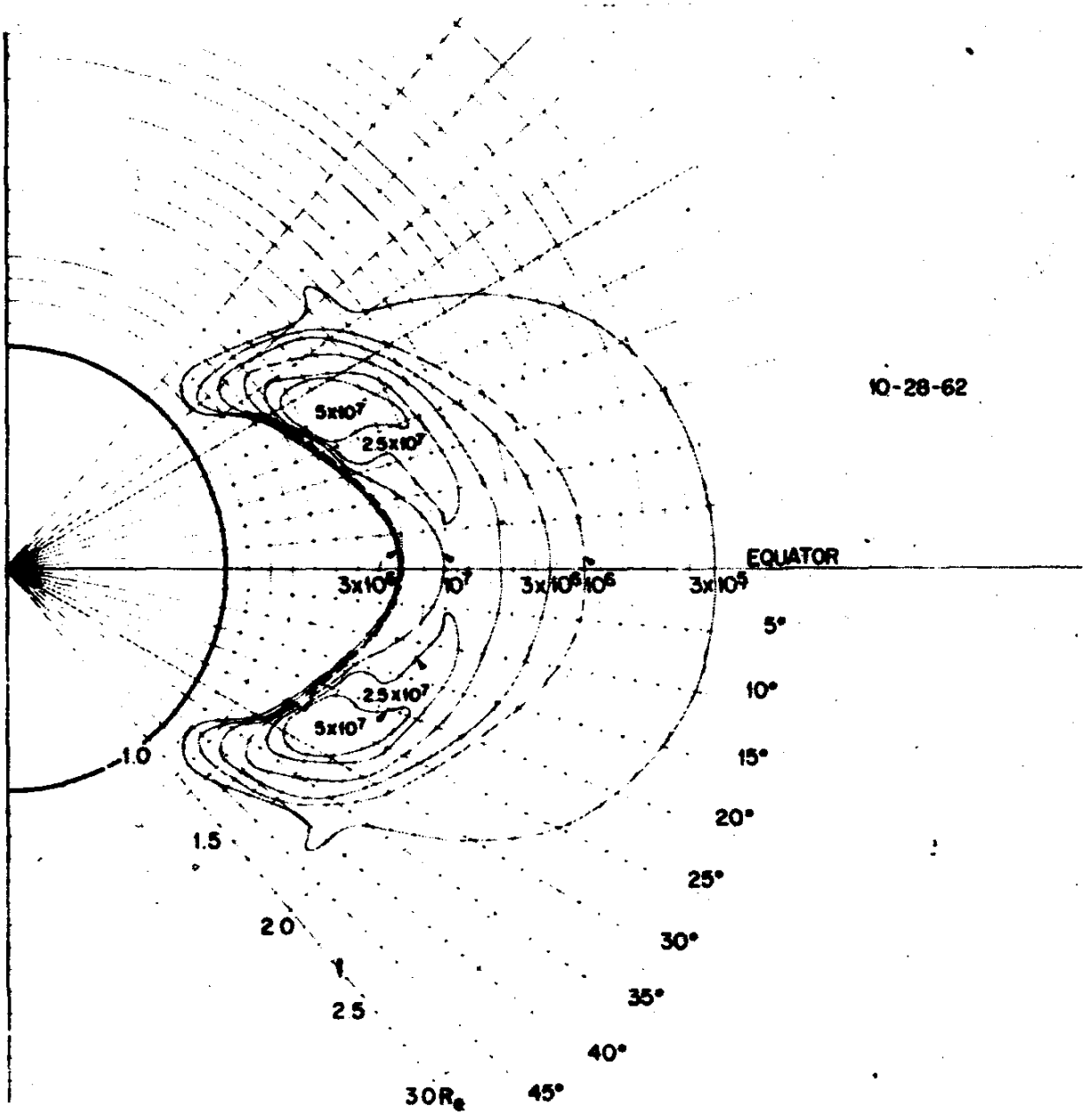

Figure 6-24. Omnidirectional flux (cm^{-2} sec^{-1}) contours (Telstar data) immediately following the Russian test of 28 October 1962 (Reference 56).

ones in that the injection was confined to a narrow band centered at L = 1.766 with a full width at half maximum in the equatorial plane of about 250 kilometers. The best readily available data describing the narrow band and its subsequent decay are given in Reference 23.

No pitch angle distributions have been published, but the observed B-independence of the omnidirectional flux measured by Explorer 15 implies (with some uncertainty) that injection occurred along the entire field line.

in the geometric factor of Telstar, the ratio of inventories for the 22 October and 28 October tests obtained by Telstar should be accurate. This ratio is about 3. The ratio of the 22 to 28 October test as computed from Alouette is also 3, although this agreement is probably fortuitous.

For the 28 October detonation, the inventory of $\sim 1.2 \times 10^{25}$ electrons appears to be the most accurate. This figure was obtained independently by two groups (References 38 and 39), using different instruments. Although West's three inventory determinations scatter by a factor of 2, the value associated with a threshold of 1.0 MeV was selected since the background is lowest at that energy. This inventory value obtained from Starad is in rather good agreement with the Telstar result of 1.6×10^{25}, a fact that supports the Telstar figure for the 22 October explosion. Since the absolute values of the Starad fluxes are probably better than those of Telstar, the Starad value for the 28 October test is accepted and the Telstar ratio of 22 to 28 October inventories is used to find the inventory for the 22 October explosion. The final results for total electron inventories, $E > 0$ are:

- Event 1—22 October, 3.6×10^{25} electrons
- Event 2—28 October, 1.2×10^{25} electrons
- Event 3—1 November, 1.2×10^{24} electrons .

The low values for inventories deduced from Alouette were disregarded because the low-altitude orbit did not sample the intense fluxes and because of uncertainties in the geometric factors. The assumption used in the inventory calculation (flux at constant-L is independent of B) is obviously wrong on the basis of the Telstar distributions.

A substantial disagreement still remains between the values from Explorer 14 and the final values selected, the difference being a factor of 8 for Event 1 and a factor of 3.5 for Event 2. In the case of Event 2, the concentration of flux off the equatorial plane (Figure 6-24) would result in a lower inventory being measured by Explorer 14. The discrepancy for Event 1 still is unresolved. However, since the Telstar orbit is much superior for sampling the artificial belt, the Explorer 14 data have been ignored in computing inventories.